# Magnetic docking stations for remotely powered light emitting diodes

*L.E. Helseth and H.Z. Wen*

*Department of Physics and Technology, Allegaten 55, 5020 Bergen, University of Bergen, Norway*

ABSTRACT: Light emitting diodes are efficient light sources which due to low power consumption often are considered for demonstrations of wireless energy transmission. It is often not only necessary to power these light sources wirelessly, but also to ensure that they conveniently dock at the correct position as effortlessly as possible without the need for chemical adhesives or mechanical attachment. In the current work a passive magnetic docking system which aids attachment of wirelessly powered light emitting diodes is proposed. The spatial range of the magnetostatic interactions is controlled by the specific magnet arrangement used, such that the light is turned on either before or after docking is initiated. The constant and time-varying magnetic fields occupy the same volume, thus allowing the presenter to demonstrate the difference between magnetostatic interactions locking the light emitting diode in place and electromagnetic induction turning the light emitting diode on.

KEYWORDS: Light emitting diode, magnetic docking, wireless

## 1. Introduction

Magnetic induction plays an increasing role in wireless power transfer and communications both in air and under water [1-7]. Meanwhile, electromagnetic induction and wireless power transfer are two phenomena often demonstrated in educational settings, either in class or as a part of lab courses [7-11]. During a demonstration, one is often interested in leaving a visual impact, for example a light emitting diode (LED) turning on [7]. Moreover, if only limited time is available for the demonstration, one may also be interested in fail-safe operations such that LED locks in place without the demonstrator having to move the coils around to find the optimal spot. With this in mind, we here demonstrate the construction of two different static magnetic docking systems for fixing small wirelessly powered LEDs. The wireless powering is facilitated by electromagnetic induction, which has a spatial range completely independent of the static magnetic forces. Emphasis is put on analyzing different simple and practical magnetic arrangements that control the spatial range of the magnetic forces acting on the unit, such that one can control whether the LED turns on before or after the system is attached to the magnets.

## 2. Magnetic docking to a combined electromagnetic coil and permanent magnet

The basic idea of wireless powering of a light emitting diode (LED) is shown in fig. 1 a). A signal generator sends a signal into a transmitting coil with frequencies in the range 0.1 kHz - 10 kHz. The resulting oscillating electromagnetic field induces a signal in another electromagnetic coil connected to an LED, thus causing this to light up. This standalone light unit (SLU) is encapsulated in a transparent isolator to make it waterproof without hindering the received electromagnetic signal. A picture of such a setup of is shown in fig. 1 b).

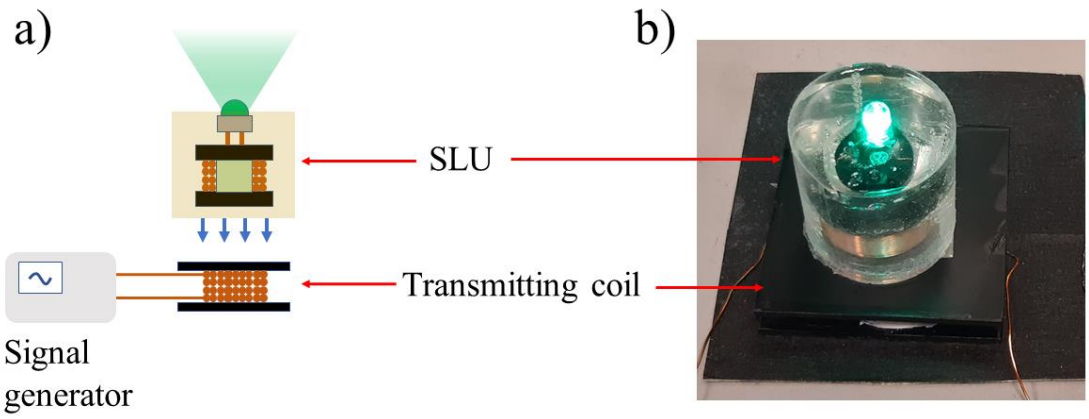


**Figure 1.** A schematic drawing of the experimental setup for wireless powering of a light emitting diode (a) together with a picture of an actual system (b). The blue arrows indicate the force acting on the standalone light unit (SLU).

The idea is to use permanent NdFeB magnets either inside the SLU unit or as a part of the transmitting coil to create a static magnetic force which attracts the SLU unit when it comes sufficiently close. The magnetic force range can be designed to be shorter or longer than the wireless powering range, according to whether the demonstrator want the LED to turn on before or after the SLU locks in place. Some demonstrators would prefer the latter, as one then could hold the SLU in midair while the LED shines. However, for other demonstrations it might be advantageous that the viewer observes that the LED turns on just as the SLU locks in place.

### 3. Magnetic docking to a combined electromagnetic coil and permanent magnet

In the first design considered, the docking of the SLU was facilitated by a strong static magnetic field generated by cylindrical permanent magnets mounted in the external docking station. The cylindrical NdFeB magnets were 2.5 mm thick, had a diameter of 10.0 mm and were purchased from the local hardware store.

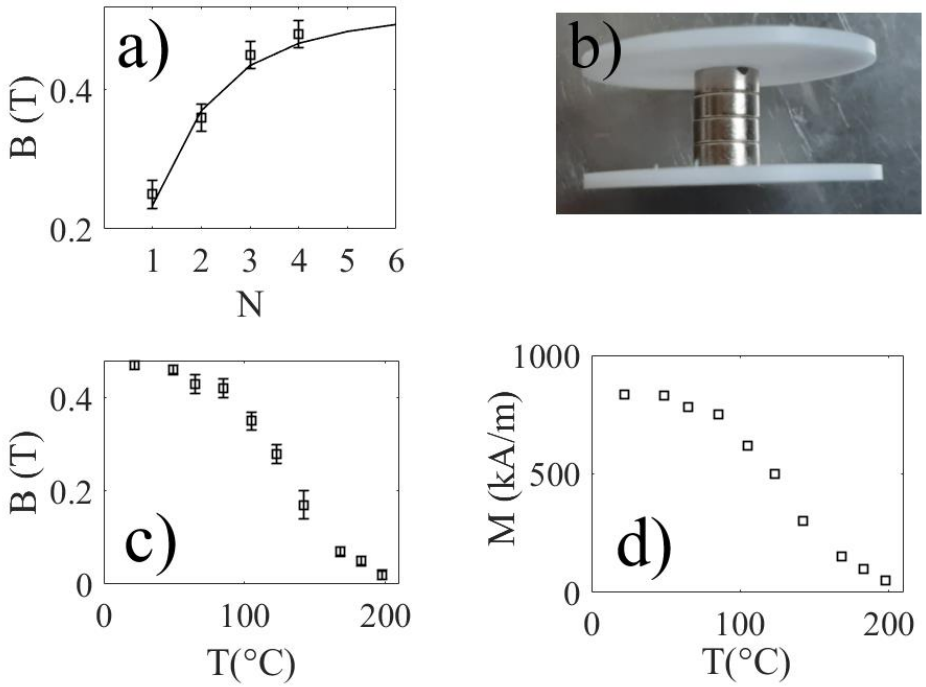


**Figure 2.** In a), the magnetic flux density is measured at the top surface as a function of number of stacked NdFeB magnets (squares). The solid line shows finite element simulation of the magnetic field versus number of magnets. In b), 4 NdFeB magnets of the magnet-based coil used for docking which form the base on which the transmitting coil is wrapped. In c), the measured magnetic field as a function of temperature on top of a stack of 4 NdFeB magnets is shown, whereas d) shows the corresponding magnetization extracted using finite element simulations.

In order to get as strong magnetic flux density as possible at the surface, the magnets were stacked on top of each other. In this way one obtained a flexible and cost-effective method to control the static field without the need for custom magnet design. The resulting magnetic flux density at the surface of the uppermost magnet was measured by a Hall probe and is shown in fig. 2 a) as squares, where N is the number of stacked magnets.

The magnetic field from a permanent magnet can be modelled either using analytical formulas or a finite element approach. Analytical models work very well for simple geometries, while more complex

geometries encompassing different elements may benefit from numerical simulations. Here, emphasis is on construction of a practical system and we have therefore chosen finite element simulations since it was available to us and was in this particular situation considered the most cost-effective method to simulate the system encompassing both permanent magnets and soft ferrites in complex geometries. For this reason, all further modelling is undertaken using finite elements. Finite element simulations were made in COMSOL 5.4 assuming that the NdFeB magnets were homogenously magnetized with saturation magnetization $M_s$=0.8 MA/m. The results are shown as a solid line in fig. 2 a). The simulations appear to fit the experimental results well, and also suggest that for N>4 the magnetic flux density does not change much with increasing N. To keep the dimensions of the docking station down, it was therefore decided to create a transmitting electromagnetic coil based on N=4 magnets as shown in fig. 2 b).

Since an electromagnetic coil was to be surrounding the magnet design in fig. 2 b), one could expect an increase in temperature when current was passed through the coil. It is well known that NdFeB magnets have rather low Curie temperature, which may influence the performance if the magnet is heated during operation. The temperature-dependent magnetization depends on the specific manufacturing procedure, and these data are usually not reported by the vendor. It was therefore deemed necessary to do a characterization of the magnetic flux density as a function of temperature. This was done by positioning the arrangement of N=4 magnets on a hot plate, and gradually increase the temperature while intermittently probing the surface magnetic flux density using the Hall probe. The corresponding magnetization plotted in fig. 2 d) was found by a finite element calculation in COMSOL 5.4 where the given magnetic flux density was used as input. The results are shown in fig. 2 c), and it is seen that the magnetic flux density and magnetization only changes very little until about 50 ˚C. In all cases reported subsequently, the temperature during device operation remained below 40 ˚C, which suggests that changes in magnetization would not be influencing the performance of the docking station.

In order to be able to generate a time-varying magnetic field, about 200 turns of insulated copper wire of resistivity $1.7 \cdot 10^{-8}$ Ωm and diameter 0.4 mm were wrapped around the four NdFeB magnet. The resulting coil was measured, using a H8118 LCR bridge, to have a resistance (1.4±0.1) Ω and inductance (0.32±0.1) mH with an outer diameter of 20 mm. The receiving system to be docked onto this combined electromagnetic coil and permanent magnet was a standalone light unit (SLU) consisting of a light emitting diode (LED) and an inductor. The LED was soldered to the leads of a commercial ferrite inductor of inductance L = (5±1) mH and R = (4±1) Ω. The inductor and LED were encapsulated in polydimethylsiloxane (PDMS) in order to make the SLU waterproof and at the same time transparent such that the ferrite inductor and the LED wires can be observed directly.

The docking of the SLU is governed by the magnetic force acting on the ferrite inductor by the stacked magnet array inside the transmitting coil. Figure 3 a) shows a finite element simulation of the magnetic flux density when the magnetization of the NdFeB magnets are $M_s$=0.8 MA/m with a NdFeB has relative permeability of 1.05. The relative permeability of the ferrite inductor is set to be $\mu_r$=1300. Only the ferrite inductor encapsulated in PDMS, and not the LED, was included in the simulation in fig. 3 a). The reason for this is that no significant force is acting on the LED. The arrows show the magnetic field lines, and the colors are associated with the value of the magnetic flux density. The magnetic force acting on the ferrite, and therefore also the entire SLU, was measured using a force sensor (Vernier dual range force sensor, range 20 N and resolution 0.01 N). The setup is shown in the inset of figure 3 b), and the corresponding experimental data are displayed as blue squares in fig. 3 b). The circles connected by a black solid line in fig. 3 b) correspond to finite element simulations of the magnetic force using the same magnetization and relative permeability as in fig. 2 a). The simulations fit well with the experimental data, with only one fitted parameter (the relative permeability of the ferrite), except for some data points in a small region near 2 mm. Both measurements and simulations were repeated numerous times to ensure that the deviations do not lie in systematic measurement errors due to factors such as accidental tilting or

temperature variations, but the reason for this deviation could not be found. It could be speculated that the magnetic properties of the ferrite inductor were not as homogenous as assumed, but we are not able to check this assumption experimentally.

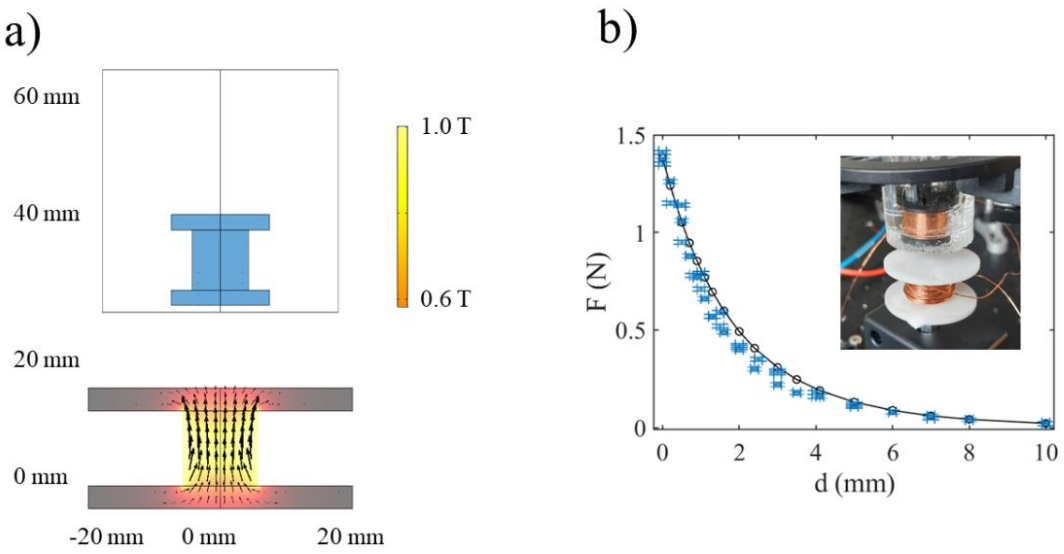


**Figure 3**. In a), a finite element simulation of the magnetic field is shown. Only the ferrite inductor encapsulated in PDMS, and not the LED, is shown in the SLU located between 30 mm and 65 mm. In b), the graph shows the measured force as a function of distance (blue points with error bars) as well as the corresponding finite element simulations in COMSOL (black circles connected by a solid line). The inset shows a picture of the measurement setup used to measure the force as a function of distance.

**4. Magnetic docking to a soft ferromagnet using a magnetic ring-arrangement**

Due to the magnetic arrangement into a rod, the docking system described in the previous section provides a relatively long-range magnetic force. However, in some cases it is necessary to provide as short range as possible such that the SLU is turned on before the docking starts. We therefore set a design goal to

create a system that generated the same magnetic maximum force as the hybrid coil in the previous section, but at the same time as short as possible magnetostatic interaction length. These two design constraints were found to be fulfilled be modifying the SLU and the transmitting coil a bit. We reason that a short magnetostatic interaction range can be facilitated by a ring-arrangement of magnetic spheres around the rim of the SLU-inductor. An added advantage is that magnets arranged in a ring with magnetization head-to-tail allow simple self-assembly since they tend to snap into place on the ferrite inductor.

We therefore decided to simulate the magnetic fields and forces as shown in fig. 4. The simulations suggest a short range magnetic interaction can be obtained by arranging spherical magnetic balls into a loop as shown in fig. 4 a). The SLU was now made slightly different from that described in the previous section. Around the perimeter of the ferrite inductor, 11 spherical NdFeB magnets of diameter 5 mm were attached with their magnetization head-to-tail as shown in fig. 4 a). An LED was soldered to the leads of a ferrite inductor, and the magnets, inductor and LED were encapsulated in polydimethylsiloxane (PDMS) in order to make the system waterproof. Now, the SLU unit had permanent magnets, and there was no need to incorporate permanent magnets in the transmitting coil. The transmitting coil had outer diameter about 40 mm and consisted of about 250 turns of copper wire of resistivity $1.7 \cdot 10^{-8}$ Ωm, had resistance 2.0 Ω, inductance 1.2 mH and diameter 0.5 mm turned around a plastic cylindrical core. In order to attract the SLU, two flat sheets of iron-nickel alloy, both 0.1 mm x 8 mm x 20 mm, were glued a distance 18 mm (center-to-center) apart on the surface of the acrylic base of the transmitting coil. The two sheets are shown as grey rectangles under the spherical magnets in fig. 4 a).

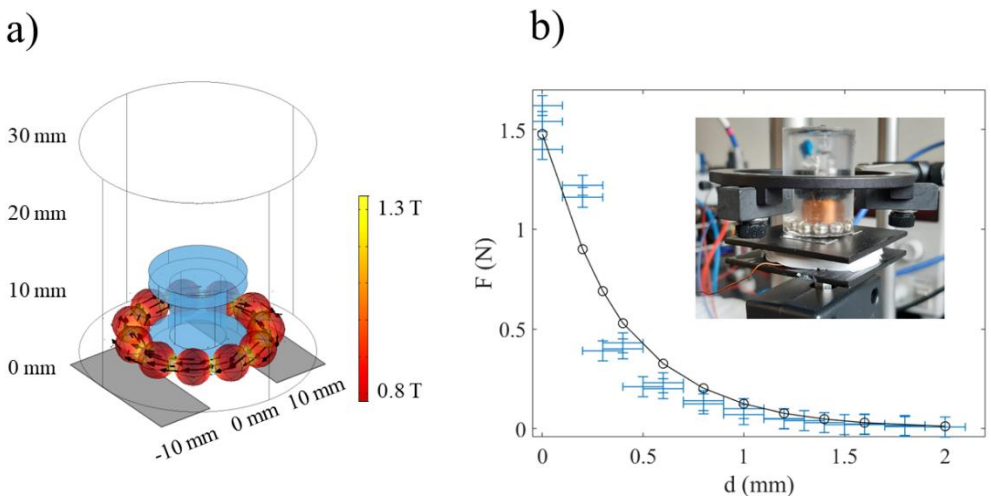


**Figure 4**. In a), a finite element simulation of the magnetic field is shown, with the arrows representing the magnetization direction along the spherical magnets. Only the ferrite inductor encapsulated in PDMS, and not the LED, is shown in the SLU. In b), the graph shows the measured force as a function of distance (blue points with error bars) as well as the corresponding finite element simulations in COMSOL (black circles connected by a solid line). The inset shows a picture of the measurement setup used to measure the force as a function of distance.

The magnetic force acting on the ferrite pieces from the SLU was measured using the same force sensor as in fig. 3 b). A picture of the setup is shown in the inset of fig. 4 b), and the corresponding experimental data are displayed as blue squares in fig. 4 b). The circles connected by a black solid line in fig. 4 b) is a finite element simulation of the magnetic force. Here it was assumed that the magnetization of the ball magnets was the same as cylindrical magnets in fig. 2 a), and that each ball had a uniform magnetization distribution. Moreover, the relative permeability of the ferrite in the inductor was also the same as in fig. 2 a), while the sheets of iron-nickel alloy had a relative permeability of 6. It is seen that there is reasonable overlap between the experimental data and the finite element simulations, with some deviations which origin could not be revealed. Comparing fig. 3 b) and 4 b), it is noticed that both arrangements generate about the same force, as required by the initial design. However, while in the former case the magnetostatic force can be measured up to about 10 mm, with the magnetic ring arrangement in fig. 4 a)

it can only be measured to about 2 mm. Thus, the close-looped spherical magnet arrangement does significantly shorten the magnetostatic interaction range.

**5. Comparison of magnetostatic docking and power transfer zones**

It is of interest to compare the range of the magnetostatic docking zone reported in the previous two sections with power transfer zone wherein wireless powering of the LED can be achieved. In order to characterize this power transfer zone, the power of the light emitted by the LED was monitored at a fixed distance from a silicon detector as shown in fig. 5 a).

The SLU reported in section 3 was clamped in a holder which could be translated in two perpendicular directions as shown in fig. 5 a). Here, *d* is the distance between the transmitting coil (A) and the back-surface of the ferrite inductor (B). The LED (C) illuminates a silicon detector (Thorlabs S120V silicon detector), and the optical power is read out by meter as the distance is varied. The transmitting electromagnetic coil was driven by a signal generator (TTI TG2000) connected to an amplifier by frequencies in the range 0-10 kHz. The frequency was tuned from 0-10 kHz, and it was found that above 2 kHz the detected light power on the silicon detector remained nearly constant. Hence, a frequency f=2.4 kHz and a peak-to-peak voltage $U_{pp}$=6 V was used to drive the transmitting coil while the distance *d* was varied. The normalized optical power as a function of distance is shown in fig. 5 b) as black squares when the whole system is in air. The container surrounding the setup was then filled by water (2.4 litres) before adding 139 g NaCl to give 58 g/L salt solution. The brown circles in fig. 5 b) show measurement of the LED-emitted light in a quiet salt solution.

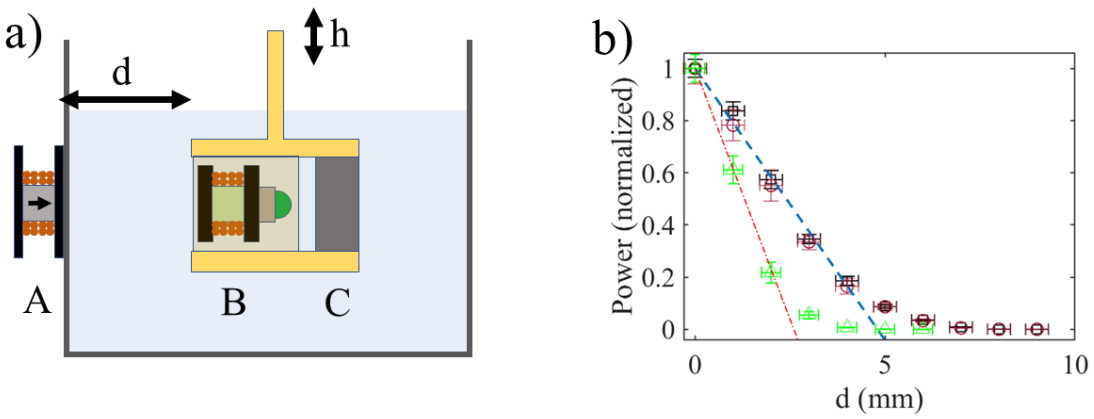


**Figure 5.** In a), a schematic drawing of the experimental setup is shown, where A is the transmitting coil (here with a NdFeB magnet in the core as in section 3), B is the SLU and C is the silicon detector. In b) the optical power received by the silicon detector is plotted as a function of distance between the encapsulated ferrite coil and the transmitter coil. The distance between the light emitting diode and the silicon detector is kept constant. The black squares correspond to measurements in air, while the brown circles correspond to 1 M NaCl for the design described in section 3. The green triangles (Δ) are measurements in air using the design described in section 4. The dashed lines are linear fits to the experimental data.

It is seen from fig. 5 b) that the distance-dependence of the optical signal received by the detector does not depend on whether the standalone light unit is immersed in air or salt water. In both cases a linear fit to the normalized power $P/P_0 = 1-d/4.8$ is a good fit to the experimental data for $d < 5$ mm, as seen from the blue dashed line in fig. 5 b). We first note that the induced voltage $U_2$ in the coil connected to the LED is $U_2=-M_{12}dI_1/dt$, where $M_{12}$ is the mutual inductance and $I_1$ is the current in the transmitting coil. The mutual inductance decreases with distance $d$ according to $1/(d+d_0)^3$ in the dipole approximation, where $d_0$ is a constant of the order of the radius of the coils used. The electrical power then decreases as the square of the voltage, i.e. $1/(d+d_0)^6$. For $d << d_0$, it is seen that the dipole coupling decreases approximately as $1-6d/d_0$. Since $d_0$ is of the order of 30 mm (the average diameter of the transmitting

coil), and $d_0/6 \approx 5$ mm, the theoretical expression $1-6d/d_0$ is in reasonable agreement with the fit to the observations found to be $1-d/4.8$.

The fact that adding salt does not change the power transfer range is due to the large skin depth given by $\delta = 1/\sqrt{\pi f \mu \sigma}$, where f is the frequency, $\mu$ is the permeability and $\sigma$ is the conductivity of the surrounding medium. For salt water $\delta \approx 5$ m, which suggests that electrical conductivity-induced eddy current damping is of negligible importance as long as the power transfer zone has a range of less than 5 mm. The power transfer zone has a smaller extension than the magnetostatic docking zone, which shows that the SLU described in section 3 turns on after the magnetic docking has started.

As for the SLU reported in section 4, the power transfer zone is shorter, as shown by the green triangles in fig. 5 b). The dash-dotted line is a linear fit $1-d/2.7$, valid for distances d < 2.5 mm. The smaller power transfer zone is due to the eddy currents induced in the conducting NdFeB ball magnets as well as the two flat sheets of ferrite alloy, acting to partially block the field. As described above, the transmitting coil used was altered to increase the signal such that the available electrical power delivered to the LED became comparable to that reported for the other SLU in the previous section. Comparing the power transfer zone with the magnetostatic docking zone, it is found that this SLU will turn on right before the docking force can be noticed by the hand.

## 6. Conclusion

In this work, it is demonstrated that magnetostatic docking of wirelessly powered, standalone light units can be facilitated by proper design of magnetostatic fields. The magnetostatic docking can be designed to be undertaken before or after the light is turned on by the electromagnetic field, and the work presented here may aid the design of more effective ways to dock remotely powered indoor or underwater lightning systems. In educational demonstrations, the presented system allows one to demonstrate the difference between magnetostatic interactions locking the light emitting diode in place and electromagnetic induction turning the light emitting diode on.

**REFERENCES**


(1) G.A. Covic and J.T. Boys, “Modern trends in inductive power transfer for transportation applications”, IEEE Journal of Emerging and Selected Topics in Power Electronics, 1, **2013**, 28-41.

(2) I.F. Akyildiz, P. Wang Z. Sun, “Realizing underwater communication through magnetic induction”, IEEE Communications Magazine, 53, **2015**, 42-48.

(3) Y.Li, S. Wang, C. Jin, Y. Zhang and T. Jiang, “A survey of underwater magnetic induction communications: Fundamental issues, recent advances, and challenges”, IEEE Communications Survey&Tutorials, 21, **2019**, 2466-2487.

(4) M. Hott and P.A. Hoeher, “Underwater communication employing high-sensitive magnetic field detectors”, IEEE Access, 8, **2020**, 177385-177394.

(5) X. Lu, P. Wang, D. Niyato, D.I. Kim and Z. Han, “Wireless charging technologies: Fundamentals, standards, and network applications”, IEEE Communications Surveys & Tutorials, 18, **2016**, 1413-1452.

(6) H.J. Kim, H. Hirayama, S. Kim, K.J. Han, R. Zhang and J.W. Choi, “Review of near-field wireless power and communication for biomedical applications”, IEEE Access, 5, **2017**, 21264-21285.

(7) J.L. Ferguson, “A supersensitive LED Faraday’s law demonstration”, Phys. Teach., 39, **2001**, 444.

(8) S.A. St. John, “Investigating wireless power transfer”, Phys. Educ., 52, **2017**, 055008.

(9) S.D. Delichte, Y.J. Lu and J.S. Bobowski, “Non-radiative mid-range wireless power transfer: An experiment for senior physics undergraduates”, Am. J. Phys., 86, **2018**, 623.

(10) K. Medjahdi, “Faraday’s law of induction by experiment”, Phys. Teach., 57, **2019**, 560.

(11) A. Bergmann, E. Dürr and C. Rockstuhl, “Wireless power transfer experiments for a high-school physics lab”, Phys. Educ. 54, **2019**, 055016.